HHS Public Access

Author manuscript

Biochemistry. Author manuscript; available in PMC 2024 July 19.

Published in final edited form as:

Biochemistry. 2018 October 02; 57(39): 5738–5747. doi:10.1021/acs.biochem.8b00817.

Molecular Insights into Human Hereditary Apolipoprotein A-I Amyloidosis Caused by the Glu34Lys Mutation

Isabel Morgado[†,‖], **Afra Panahi**[‡,▫], **Andrew G. Burwash**[‡], **Madhurima Das**[†,#], **John E. Straub**[*,‡], **Olga Gursky**[*,†,§]

[†]Department of Physiology & Biophysics, Boston University School of Medicine, Boston, Massachusetts 02118-2526, United States

[‡]Department of Chemistry, Boston University, Boston, Massachusetts 02215-2521, United States

[§]Amyloidosis Treatment and Research Center, Boston University School of Medicine, Boston, Massachusetts 02118, United States

Abstract

Hereditary apolipoprotein A-I (apoA-I) amyloidosis is a life-threatening incurable genetic disorder whose molecular underpinnings are unclear. In this disease, variant apoA-I, the major structural and functional protein of high-density lipoprotein, is released in a free form, undergoes an α-helix to intermolecular cross-β-sheet conversion along with a proteolytic cleavage, and is deposited as amyloid fibrils in various organs, which can cause organ damage and death. Glu34Lys is the only known charge inversion mutation in apoA-I that causes human amyloidosis. To elucidate the structural underpinnings of the amyloidogenic behavior of Glu34Lys apoA-I, we generated its recombinant globular N-terminal domain (residues 1–184) and compared the conformation and dynamics of its lipid-free form with those of two other naturally occurring apoA-I variants, Phe71Tyr (amyloidogenic) and Leu159Arg (non-amyloidogenic). All variants showed reduced structural stability and altered aromatic residue packing. The greatest decrease in stability was observed in the non-amyloidogenic variant, suggesting that amyloid formation is driven by local structural perturbations at sensitive sites. Molecular dynamics simulations revealed local helical unfolding and suggested that transient opening of the Trp72 side chain induced mutation-dependent structural perturbations in a sensitive region, including the major amyloid hot spot

[*]Corresponding Authors: Boston University School of Medicine, W302D, 700 Albany St., Boston, MA 02118. gursky@bu.edu. Boston University, 590 Commonwealth Ave., Boston, MA 02134. straub@bu.edu.

[‖]**Present Addresses:** I.M.: Stanford Cardiovascular Institute, Stanford University School of Medicine, Palo Alto, CA 94304.

[▫] **Present Addresses:** A.P.: Department of Chemistry and Biochemistry, California State University, San Marcos, CA 92096.

[#]**Present Addresses:** M.D.: Simon-Kucher & Partners, Cambridge, MA 02141.

Author Contributions

A.P. and I.M. contributed equally to this work. Study concept, design, and supervision: O.G. and J.E.S. Acquisition of data: I.M., M.D., A.P., and A.G.B. Analysis and interpretation of data: I.M., A.P., A.G.B., O.G., M.D., and J.E.S. Drafting of the manuscript: A.P., I.M., J.E.S., and O.G.

The authors declare no competing financial interest.

ASSOCIATED CONTENT

Supporting Information

The Supporting Information is available free of charge on the ACS Publications website at DOI: 10.1021/acs.biochem.8b00817. Characterization of recombinant globular domains of apoA-I (residue fragments 1–184) used in this study (Figure S1), root-mean-square deviation from the initial structure of C_α atomic positions as a function of simulation time (Figure S2), and probability distribution of dihedral angles χ_1 and χ_2 for Trp8, Trp50, and Trp108 in WT and variant apoA-I (Figure S3) (PDF)

residues Leu14–Leu22. We posit that a shift from the “closed” to the “open” orientation of the Trp72 side chain modulates structural protection of amyloid hot spots, suggesting a previously unknown early step in the protein misfolding pathway.

Graphical Abstract

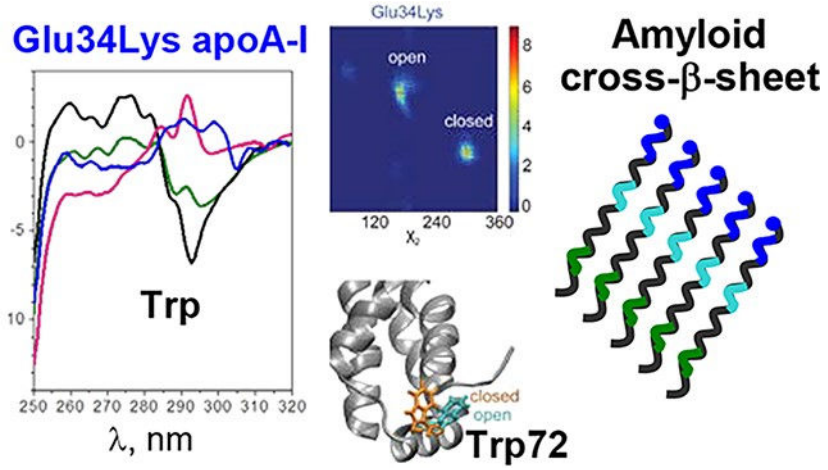

Amyloid diseases, including neurodegenerative and systemic amyloidoses, affect millions of patients worldwide and are a major public health challenge. The hallmark of this group of diverse diseases is misfolding of a protein, from its native conformation into an intermolecular cross-β-sheet, leading to deposition of insoluble amyloid fibrils in organs and tissues.

Apolipoproteins (apos) make up a family of lipid surface binding proteins overrepresented in amyloidosis.[1,2] Human apoA-I (243 amino acids) is the major structural and functional constituent of plasma HDL that transports cholesterol from peripheral cells to the liver for catabolism and protects against cardiovascular disease and inflammation.[4] Numerous naturally occurring *APOA1* gene mutations lead to reduced plasma levels of HDL and apoA-I. Some mutations, such as Leu159Arg, are associated with abnormal lipid metabolism and increased risk of atherosclerosis, while others cause amyloidosis but no atherosclerosis *in vivo*.[5] The molecular basis for this clinical presentation is unclear and is being addressed in the ongoing studies of several groups, including ours.

Hereditary apoA-I amyloidosis (AApoAI) is an autosomal dominant disorder wherein mutations in the *APOA1* gene cause amyloid deposition of mainly N-terminal fragments of the variant protein in kidney, liver, heart, spleen, testicles, gastrointestinal tract, and other organs, causing organ damage and failure.[1,6] Currently, there is no targeted therapy for AApoAI. The available treatments for this life-threatening disease are limited to hemodialysis and organ transplant.[7] Approximately 20 AApoAI variants have been reported worldwide (http://www.amyloidosismutations.com), with mutation sites located in two regions. “Inside” mutations cluster in residues 26–107 from N-terminal 9–11 kDa segments that form fibrillar deposits in AApoAI, while “outside” mutations cluster in residues 154–178.[6,8,9] Notably, all known amyloidogenic mutations are located in the N-terminal domain

of apoA-I (residues 1–184), suggesting that protein misfolding is triggered by the perturbed conformation of this globular domain.[9]

Human apoA-I contains two structural domains, an N-terminal domain (residues 1–184) that forms a globular four-helix bundle in a lipid-poor/free protein in solution and a flexible hydrophobic C-terminal tail (residues 185–243) that contains a primary lipid binding and aggregation site (ref 10 and references therein). These domains undergo large conformational changes upon reversible binding to the lipid surface.

Most circulating apoA-I (~95%) is bound to the HDL surface in a highly α-helical "double belt" or a related conformation and is stabilized by high kinetic barriers that protect the protein from aggregation and misfolding in amyloid (refs 2, 3, 9, and 11 and references therein). However, a small fraction of apoA-I can be transiently released from HDL in a labile globular lipid-poor/free state (termed "free" for the sake of brevity) that is proposed to form the protein precursor of amyloid.[2,11] The 2.2 Å resolution X-ray crystal structure of the globular domain, Δ(185–243) apoA-I, crystallized as a dimer, is the only currently available high-resolution structure of lipid-free apoA-I[10,12] (Figure 1).

Although the atomic structure of full-length lipid-free apoA-I is currently not available, strong evidence suggests that the C-terminal tail wraps around the four-helix bundle seen in the crystal structure and probably interacts weakly with the hydrophobic cleft between the two pairs of helices (Figure 1, short arrow).[12,13] Because the conformations of this four-helix bundle in the full-length wild type (WT) protein and in its C-terminally truncated residue fragment 1–184 encompassing the globular domain are very similar, the globular domain provides a useful model for understanding the structure of full-length WT.[10,14–16] In fact, multiple lines of evidence suggest that the secondary and tertiary structure and stability of the N-terminal domain remain essentially invariant upon truncation of the C-terminal tail. This is indicated by far-ultraviolet (UV) and near-UV circular dichroism (CD) spectroscopy (the latter is exquisitely sensitive to Trp packing in the N-terminal domain) and by the agreement between the X-ray crystal structure of this domain and the secondary structural assignments in the full-length apoA-I monomer in solution by hydrogen–deuterium exchange mass spectrometry.[10,17] Importantly, the N-terminal domain contains all known sites of AApoAI mutations, three of four amyloidogenic segments, and the 9–11 kDa N-terminal fragments found in AApoAI deposits *in vivo*.[9,18,19] Therefore, its X-ray crystal structure provides an excellent starting model for understanding what makes apoA-I amyloidogenic.[9] This model was used in the current study (Figure 1).

Previous biophysical and bioinformatic studies of several disease-causing apoA-I variants have postulated that amyloidogenic mutations perturb the native packing in the globular domain, thereby increasing the solvent exposure of the major amyloid "hot spot" residues 14–22; the increased exposure of this adhesive segment was proposed to trigger protein misfolding from its native highly α-helical conformation into an intermolecular cross-β-sheet in amyloid (refs 18 and 19 and references therein). The exact molecular events whereby the mutations trigger apoA-I misfolding remain unknown. Identifying such early events in the misfolding pathway of this or other amyloidogenic proteins may help improve therapeutic targeting of the hitherto incurable amyloid diseases.

Here, the focus is on the Glu34Lys mutation, which causes severe systemic amyloidosis in the third and fourth decades of life involving kidney, liver, eyes, testicles, and other organs.[8,20] This debilitating life-threatening disease culminates in kidney failure, necessitating organ transplant.[7] Unlike other AApoAI variants, Glu34Lys is the only known charge inversion variant and the only *APOA1* mutation located at the "top" of the four-helix bundle in lipid-free protein (Figure 1). To elucidate the molecular basis for the amyloidogenic behavior of Glu34Lys apoA-I *in vivo*, we generated its recombinant globular domain and explored its conformation, stability, and dynamics *in vitro* and in silico. As controls, in addition to WT apoA-I, we chose two naturally occurring variants with different biophysical properties and clinical presentations. Phe71Tyr is the most conservative AApoAI mutation that minimally perturbs the protein structure *in vitro*;[12,19] *in vivo*, it is associated with mild AApoAI restricted to amyloid in the palate.[8] In contrast, the Leu159Arg mutation, which greatly perturbs the protein structure *in vitro*,[19] is non-amyloidogenic but causes aberrant lipid metabolism and an increased risk of cardiovascular disease, and the variant protein is rapidly degraded *in vivo*.[5,21] Biophysical and structural studies of these variants provide new insights into the early steps of the misfolding pathway of Gly34Lys, Phe71Tyr, and perhaps other disease-causing protein variants.

MATERIALS AND METHODS

Recombinant Proteins: Construct Design, Expression, and Purification.

The coding sequences for the globular domains of human apoA-I (residue fragment 1–184) WT, Gly34Lys, Phe71Tyr, and Leu159Arg, were synthesized and cloned into the pMAL-c4X vector (GenScript). The gene synthesis and cloning system was customized to insert a six-His tag followed by the cleavage sequence for tobacco etch virus protease immediately after the C-terminus of the maltose binding protein (MBP) and before the N-terminus of apoA-I. This enabled us to use His-tag affinity chromatography followed by MBP removal to obtain pure proteins containing no additional N-terminal residues. The constructs were transformed into *Escherichia coli* BL21(DE3) CodonPlus-RIL (Stratagene) using the heat-shock method, and the cells were selected by the resistance to ampicillin (100 μg/mL) in lysogeny broth agar plates. To overexpress each protein, a single colony was inoculated in 25 mL of LB ampicillin (100 μg/mL) and incubated overnight in a shaker at 37 °C and 250 rpm. The preculture was used to inoculate 1 L of lysogeny broth ampicillin (100 μg/mL) and grown in a shaker at 37 °C and 250 rpm until the OD_{280} reached ~0.5. Protein expression was induced with 1 mM isopropyl 1-thio-D-galactopyranoside, and bacteria were incubated for 4 h at 30 °C in a shaker at 250 rpm. Cells were harvested by centrifugation at 14000g for 20 min, resuspended in binding buffer [50 mM sodium phosphate, 150 mM NaCl, and 10 mM imidazole (pH 8.0)], and stored at −20 °C.

For protein purification, the cell pellet was thawed on ice, resuspended in 40 mL of binding buffer supplemented with cOmplete, EDTA-free protease inhibitor cocktail (Roche), and sonicated thrice for 20 s to lyse the cells. The cell extract was centrifuged at 25000g and 4 °C for 30 min with 5% polyethylenimine to precipitate DNA. The supernatant was passed through a 0.22 μm filter, loaded on a 5 mL His-Trap column connected to an ÄKTA fast protein liquid chromatography system (GE Healthcare), and pre-equilibrated

with binding buffer. After being washed with 5 column volumes of wash buffer [50 mM sodium phosphate, 150 mM NaCl, and 20 mM imidazole (pH 8.0)], the sample was eluted with elution buffer [50 mM sodium phosphate, 150 mM NaCl, and 250 mM imidazole (pH 8.0)]. The fractions containing the pure MBP-His–apoA-I fusion protein were pooled; tobacco etch virus protease was added at a 1:50 TEV:protein molar ratio, and the mixture was incubated at 4 °C for 16 h. The digested mixture was transferred to binding buffer using centrifugal filter units (Amicon, Millipore) and run through the 5 mL His-Trap column. The apoA-I fractions were recovered in the flowthrough, while the MBP-His fragment was retained in the column.

ApoA-I fractions were assessed by sodium dodecyl sulfate polyacrylamide gel electrophoresis (SDS–PAGE) (14% acrylamide Tris-Glycine, Denville blue protein stain). Pure fractions that migrated as a single band at ~22 kDa were collected and used for biophysical studies. The protein identity and purity were confirmed by intact mass check using electrospray ionization mass spectrometry–reverse phase liquid chromatography (Figure S1A,B).

Size-Exclusion Chromatography (SEC).

The oligomeric state of purified apoA-I variants was determined by SEC using a Superdex 200 10/300 GL column connected to an ÄKTA fast protein liquid chromatography system (GE Healthcare). To calibrate the column, 200 μL of a sample containing protein standards from the Gel Filtration Calibration Kit (GE Healthcare) was injected: apoferritin (443 kDa), conalbumin (76 kDa), cytochrome c (12.4 kDa), aprotinin (6.5 kDa), and vitamin B_{12} (1.35 kDa). The calibration plot for standards was created according to the manufacturer's protocol and used to calculate the apparent mass of self-associated apoA-I by interpolation. ApoA-I variants were transferred to running buffer (10 mM sodium phosphate and 150 mM NaCl) using centrifugal filter units (Amicon, Millipore) and loaded individually on the column (100 μL sample of 0.2–0.5 mg/mL protein). Each sample was analyzed at a flow rate of 1 mL/min. Protein elution was monitored by the absorbance at 280 nm (Figure S1C,D) using UNICORN software (GE Healthcare).

Circular Dichroism (CD) Spectroscopy.

CD data were recorded by using an AVIV 400 spectropolarimeter (Aviv Biomedicals). To characterize protein secondary structure, far-UV CD spectra were recorded at 190–250 nm with a 1 nm step size using samples (~0.1 mg/mL protein in standard buffer) placed in 1 mm path-length cells. The data were normalized to protein concentration and reported as molar residue ellipticity, [Θ]. The protein α-helical content was determined from the CD signal at 222 nm, $[\Theta]_{222}$, as previously described;[22] the standard error in this estimate was ±5%. The protein stability was assessed by thermal denaturation wherein samples were heated and cooled from 25 to 90 °C at a constant rate of either 10 or 60 °C/h, and α-helical unfolding and refolding were monitored as a function of temperature at 222 nm, $[\Theta]_{222}(T)$. The melting temperature, T_m, was determined as the midpoint of the sigmoidal unfolding transition with a standard error of ±1.5 °C. To asses effects of mutations on the aromatic packing in the apoA-I globular domain, near-UV CD spectra were recorded at 250–320 nm from samples containing ~1 mg/mL protein in standard buffer placed in a cell with a 5 mm path length

at 25 °C. Near-UV CD data were reported in units of molar ellipticity, Θ. ORIGIN software (MicroCal) was used for the data analysis and display. Except for intact mass check, all measurements of recombinant proteins were recorded three or more times from two or three biological replicates to ensure reproducibility.

Molecular Dynamics (MD) Simulations.

As a starting model, we used the monomer structure of the C-terminally truncated WT, which was built from the crystallographic dimer observed in the 2.2 Å resolution structure of human Δ(184–243) WT (Protein Data Bank entry 3R2P).[10] Following previous studies,[23] the monomer was obtained via domain swapping of one helical segment (apoA-I sequence repeats h6 and h7) around the dimer two-fold axis (Figure 1), which retains the helix bundle packing but involves rebuilding of the flexible central linker (residues 129–132) in the h5 sequence repeat. The linker was built manually by attaching the backbone of residue segment 129–132 to the adjacent backbone from helical sequence repeat h5 using the "build" module in the PyMOL 2.0 molecular graphics system (Schrödinger, LLC). The starting model contained residues 3–182 that were well-ordered in the crystal structure. This monomer structure was solvated with TIP3P water molecules and Na^+ and Cl^- ions at a concentration of 0.15 M and simulated for 400 ns at constant temperature and pressure to equilibrate the system and resolve any possible clashes between the side chains of the newly built linker and the rest of the protein. The temperature and pressure in all simulations were controlled by a Nose–Hoover thermostat and Parrinello–Rahman barostat.[23–25] The initial configurations of the solvated protein were constructed using CHARMM-GUI.[26,27] All simulations were performed using the GROMACS 5.0[28] simulation package and the CHARMM36 force field.[29] The structures were rendered in VMD.[30] The analyses were performed with codes developed in house and the MD Analysis tool set.[31]

Point substitutions Glu34Lys, Phe71Tyr, and Leu159Arg were made in the equilibrated structure to obtain starting models for the mutant proteins. For each system (WT and three mutant proteins), three sets of independent simulations were performed at 300 K and 1 bar. Each simulation ran for 290 ns, from which the last 250 ns was used for analysis. During these room-temperature simulations, the structures changed little from the original models; e.g., no significant helical unfolding was observed. This is illustrated by the root-mean-square deviations for C_α atoms (Figure S2).

To increase the rate of conformational sampling and obtain the helical content that represents closely the protein solution conformation (~60% helix measured by far-UV CD as compared to 80% in the initial model), we followed the strategy of Segrest and colleagues.[13] For each protein, the most dominant structures of the room-temperature runs were heated to 500 K over 50 ps and simulated for an additional 20 ns, from which the last 10 ns was used for analysis.

To investigate the orientation of tryptophan side chains, χ_1 and χ_2 dihedral angles of Trp72, Trp8, Trp50, and Trp108 were determined for WT, Glu34Lys, Phe71Tyr, and Leu159Arg (Figure S3). Because variations in the dihedral angles represent local structural fluctuations, room-temperature structural ensembles were used. The χ_1 angle was measured using the N, C_α, C_β, and C_γ atoms, while the χ_2 angle was measured using the C_α, C_β, C_γ, and

$C_{\delta 1}$ atoms. The angles were calculated at each step of the trajectory, and two-dimensional histograms were generated to compare the relative amount of time (i.e., steps of the trajectory) corresponding to each combination of χ_1 and χ_2.

The pairwise C_α correlation coefficients were calculated for high-temperature simulations to highlight how structural fluctuations in different parts of the protein were positively correlated or anticorrelated (correlation coefficient of 1 or −1, respectively) with respect to each other. For each variant protein, the collected average structures from the three simulation replicates were obtained and the absolute difference between the correlation coefficient of each variant and the WT was calculated to highlight the similarities and differences between the variants and the WT.

RESULTS

Disease-Causing Mutations Destabilize the Globular Domain and Alter Its Aromatic Residue Packing.

Of all naturally occurring, full-length, recombinant apoA-I variants explored to date by our team, we had experimental difficulties with only Glu34Lys. This mutation led to a greatly decreased protein yield, and the protein precipitated after cleavage of the tag, thereby precluding our attempts to obtain stable soluble full-length Glu34Lys apoA-I for biophysical studies. To bolster protein expression and solubility, the flexible hydrophobic C-terminal tail (residues 185–243) was truncated and the expression system was optimized to obtain ultrapure Δ(185–243) Glu34Lys as described in Materials and Methods. Previous biophysical studies of full-length WT, Phe71Tyr, and Leu159Arg variants[18,19] provided useful controls for the current study of the globular domains.

All proteins explored were pure and monodisperse in solution and formed dimers observed by size-exclusion chromatography (Figure S1), similar to the crystallized construct.[10] These proteins were used (i) to test whether C-terminally truncated Phe71Tyr and Leu159Arg variants provided adequate structural models for their full-length counterparts, which have been previously explored,[17,18] and (ii) to determine how Glu34Lys, Phe71Tyr, and Leu159Arg substitutions affect the structure and stability of the globular domain.

Far-UV CD spectra at 25 °C (Figure 2A) indicated an α-helical content ranging from 56 ± 5% for Δ(185–243) Glu34Lys to 62 ± 5% for Δ(185–243) WT, similar to the value of 60 ± 5% α-helix (or ~110 residues) reported previously for Δ(185–243) WT.[10] Comparison with full-length WT, which showed 50 ± 5% α-helix, including ~110 residues in the globular domain,[12] suggested that this domain had very similar secondary structure in the full-length and C-terminally truncated WT. A similar conclusion was reached for Phe71Tyr and Leu159Arg variants. In addition, like C-terminally truncated Glu34Lys protein, full-length as well as truncated Phe71Tyr and Leu159Arg proteins also showed a marginally significant helical loss upon single-amino acid substitutions (ref 19 and Figure 2A). In summary, the helical content in the globular domain was perturbed slightly by the point substitutions in this domain, such as Glu34Lys, Phe71Tyr, and Leu159Arg, but did not significantly change upon C-terminal truncation.

Near-UV CD spectra were used to probe the aromatic residue packing in the globular domain. This domain contains all four tryptophans and five of seven tyrosines in apoA-I, which dominate its near-UV CD spectrum. Importantly, globular domains of Glu34Lys, Phe71Tyr, and Leu159Arg variants showed distinctly different spectra, indicating that these point mutations altered the aromatic residue packing (Figure 2B). In addition, for WT, Phe71Tyr, and Leu159Arg proteins, globular domains and full-length protein forms showed very similar near-UV CD spectra (Figure 2B compared with Figure 2C in ref 19). Moreover, the near-UV CD spectrum of truncated and full-length recombinant WT resembled closely the spectrum of plasma lipid-free apoA-I.[10,19] These results show that Δ(185–243) truncation did not significantly change the aromatic side chain packing in the globular domain. However, this packing was altered by the point substitutions in this domain, such as Glu34Lys, Phe71Tyr, and Leu159Arg.

Protein stability was probed by thermal denaturation wherein changes in the α-helical content during heating were monitored by CD at 222 nm as described in Materials and Methods. All proteins showed a cooperative unfolding (Figure 2C) that was independent of the heating rate, indicating thermodynamic reversibility. The transition midpoint, measured with standard error of ±1.5 °C, was T_m = 57 °C in truncated WT and Phe71Tyr, significantly lower than that in full-length proteins (62 °C for WT and 60 °C for Phe71Tyr).[16] Truncated Glu34Lys showed a T_m of 52 °C (Figure 2C). Truncated Leu159Arg showed the lowest T_m of 37 °C, which was 20 °C lower than that of full-length Leu159Arg.[19] Truncated Leu159Arg also showed less cooperative unfolding, which was evidenced by a decreased slope of the melting curve (Figure 2C, pink). These results are in excellent agreement with previous spectroscopic and hydrogen–deuterium exchange studies of full-length Leu159Arg, which suggested that Arg159 perturbs the core of the four-helix bundle and splits it along the hydrophobic cleft, thus decreasing the protein's stability and unfolding cooperativity and allowing the helix bundle to better sequester the C-terminal tail.[19] As a result, deletion of the C-terminal tail causes greater destabilization of the helix bundle in Leu159Arg than in Glu34Lys or other proteins.

The rank order of the protein stability emerging from the current study is WT ≅ Phe71Tyr > Glu34Lys > Leu159Arg (Figure 2C), in agreement with that observed in full-length proteins, WT ≥ Phe71Tyr > Leu159Arg.[19] This agreement suggests that, similar to their globular domains, full-length Glu34Lys is less stable than WT and Phe71Tyr but more stable than Leu159Arg apoA-I. This result is consistent with the clinical finding that Glu34Lys mutation carriers have normal plasma levels of apoA-I and HDL, unlike Leu159Arg carriers whose plasma levels are reduced.[5,21]

In summary, our biophysical studies revealed several new findings. First, Glu34Lys charge inversion has a minimal effect on the overall secondary structure in the globular domain of apoA-I (Figure 2A) but decreases its stability, as evidenced by an ~5 °C reduction in T_m (Figure 2C). Second, point substitutions in the globular domain, including Glu34Lys, Phe71Tyr, and Leu159Arg, altered near-UV CD spectra and, hence, altered the aromatic side chain packing in the globular domain (Figure 2B and ref 19). Third, despite its destabilizing effects, the C-terminal truncation had no significant effects on the secondary structure or aromatic packing in the globular domain of WT, Phe71Tyr, Leu159Arg (Figure 2A–C), and,

by inference, Glu34Lys. These results validate the use of globular domains of these variant proteins as structural models for understanding their full-length counterparts. As such, they were employed in all molecular dynamics (MD) simulations, with initial coordinates drawn from the crystal structure of Δ(185–243) WT.[10] CD data of these globular domains of WT, Glu34Lys, Phe71Tyr, and Leu159Arg (Figure 2) provided important experimental controls for these MD simulations.

Mutations Induce Local Unfolding and Alter Protein Dynamics in MD Simulations.

To unravel early steps in the misfolding of apoA-I, we performed MD simulations of the globular domains of WT, Glu34Lys, Phe71Tyr, and L159Arg proteins using the atomic structure of Δ(185–243) WT as a starting model. We simulated the monomeric apoA-I instead of the crystallographic dimer (Figure 1) for several reasons. First, the free apoA-I monomer is thought to form a structurally labile metabolically active species that is the protein precursor of amyloid *in vivo*; this monomeric species constitutes ~5% of circulating plasma apoA-I, while the remaining HDL-bound apoA-I is stabilized by high kinetic barriers protecting the protein from misfolding in amyloid (refs 2, 3, 9, and 11 and references therein). Second, the helix bundle structure in the monomer is very similar to that of the dimer, as the two structures are related via the domain swapping of one helical segment.[10] Third, because the simulation time increases steeply with an increase in the protein size, the smaller monomer facilitated more extensive MD simulations. The monomer structure was obtained from the dimer via the domain swapping of one helical segment around the two-fold axis (Figure 1) as described in Materials and Methods.

First, the WT starting model was equilibrated at 300 K for 400 ns. Next, mutations were introduced; the structures were run at 300 K for 290 ns, and the last 250 ns was used for analysis. These room-temperature simulations were repeated thrice for each variant. The four-helix bundle in all proteins remained stable (Figure S2). To diversify the conformational sampling, the dominant structure from the room-temperature simulations of each protein was heated to 500 K over 50 ps, followed by simulation for 20 ns at 500 K. The last 10 ns portions of these high-temperature simulations were used for analysis of helicity and correlation maps (see Materials and Methods for details).

The helix bundle in WT, Glu34Lys, Phe71Tyr, and Leu159Arg proteins remained stable after high-temperature simulations but showed a decreased secondary structure content, mainly in residues 34–81 (Figure 3). Hence, the average α-helical content in the WT decreased from ~80% in the starting model to 60% in the final model. The latter agreed with the 61% α-helix content determined by CD spectroscopy in Δ(185–243) WT in solution (Figure 2) and with previous CD[10] and MD studies of this protein.[13,15] Similarly, all variant proteins showed a decrease in their helical content by ~20% due to partial unfolding of the helical structure as compared to the starting model, which was 80% α-helical (Figure 3). This result agreed with the values of 56–62% α-helix observed in these proteins in solution by far-UV CD (Figure 2).

All proteins studied here showed full or partial unfolding of residues 34–81 (Figure 3) encompassing the second helical segment from the four-helix bundle and adjacent hinge regions. The flexible secondary structure in this region is consistent with two large-scale

motions, one around the “top hinge” near residue Gly39 and another around the “bottom hinge” containing Gly65, Pro66, and nearby groups; such hinge motions were proposed to mediate helix bundle opening during binding of apoA-I to HDL.[10,14,15] A kinked α-helix at the bottom of the bundle starting at Gln69 showed partial unfolding that was particularly pronounced in Phe71Tyr variant, probably because of the local perturbation around this mutation site (Figure 3).

Despite these overall similarities, local mutation-specific differences were also observed. This included the helical conformation at Tyr18 and downstream. Tyr18, which is located near a helical kink in the middle of the bundle, is in the middle of the major amyloid hot spot segment, Leu14–Leu22 (Figure 3B). Adhesive segments such as this are normally protected by their native packing from initiating protein misfolding (ref 19 and references therein). In WT, this segment is fully helical and thus protected, yet in all three apoA-I variants, this region shows an apparent loss of helicity (Figure 3A,B). We propose that such a mutation-induced loss of structural protection in this major amyloid hot spot helps initiate apoA-I misfolding and aggregation. In fact, the structural protection observed in segment Leu14–Leu22 by hydrogen–deuterium exchange mass spectrometry declined in the order WT > Phe71Tyr > Leu159Arg.[19] Hence, partial loss of helical structure in the major amyloid hot spot of Glu34Lys, Phe71Tyr, and Leu159Arg, suggested by our MD simulations (Figure 3) and supported by experiment,[19] suggests a possible molecular basis for amyloid formation by these proteins.

To determine how single-amino acid substitutions influence concerted molecular motions in apoA-I, the pairwise correlation coefficients for C_α atoms were calculated for high-temperature structural ensembles. Figure 4A shows a correlation map for the WT; positively correlated regions move together (red), while negatively correlated regions move out of phase (blue). For each simulation, the average structure from three high-temperature replicates was calculated, and the absolute difference among Glu34Lys, Phe71Tyr, and Leu159Arg variants and the WT was mapped to illustrate mutational effects on the molecular motion (Figure 4B–D). The difference map for Phe71Tyr showed few small areas where the variant protein deviated from the WT, while Glu34Lys and, especially, Leu159Arg showed much larger deviations (Figure 4B–D). Although the detailed interpretation of these maps was outside the scope of this study, these results revealed that the effects of the point substitutions on the molecular motion were not localized to the mutation site but distributed across the protein and progressively increased from Phe71Tyr to Glu34Lys to Leu159Arg (Figure 4B–D). A similar rank order was observed for the experimentally determined thermal stability: WT > Phe71Tyr > Glu34Lys > Leu159Arg (Figure 2C).

Together, our experimental and computational results consistently show that Glu34Lys charge inversion, which is much less conservative than Phe71Tyr substitution, is also more disruptive. Notably, the most disruptive mutation, Leu159Arg, is non-amyloidogenic *in vivo*. These results support the idea that structural destabilization alone is insufficient to make apoA-I amyloidogenic and suggest that local changes in the protein conformation and dynamics in sensitive regions are important for amyloid formation by variant proteins.[19]

Amyloidogenic Mutations Induce a Conformational Shift in Trp72.

Because Glu34Lys, Phe71Tyr, and Leu159Arg variants have a distinctly different Trp side chain packing indicated by near-UV CD (Figure 2B), we analyzed MD trajectories to determine the conformational distribution of Trp in each protein. To depict local side chain motions, room-temperature trajectories were used. Dihedral angles χ_1 and χ_2 for each Trp were calculated at each step of the trajectory, and two-dimensional histograms were obtained to compare the relative time spent in any given combination of χ_1 of χ_2. ApoA-I contains four tryptophans (Trp8, Trp50, Trp72, and Trp108), one or more of which potentially contribute to the mutation-induced spectral changes in near-UV CD (Figure 2B). In the crystal structure, Trp8 and Trp72 are packed in the hydrophobic cluster at the “bottom” of the helix bundle, together with Phe71 and adjacent leucines; Trp50 forms a π-cation interaction with Lys23 in the middle of the bundle, and Trp108 together with Phe33 and Phe104 is packed in the “top” aromatic cluster.[10]

MD simulations suggested significant mutational effects on the conformation of Trp72 (Figure 5). In WT, the vast majority of Trp72 rotamers clustered in a single region near a $\chi_1 = 295°$, $\chi_2 = 120°$; this “closed” conformation represented the imidazole ring packed in the “bottom” hydrophobic cluster, similar to that seen in the crystal structure (Figure 5A). Although in mutant proteins this “closed” conformation remained predominant, its relative occupancy decreased and alternative conformations became populated (Figure 5B–D). In such “open” conformations, the imidazole ring of Trp72 pointed away from the hydrophobic cluster and into the solvent, thus allowing solvent entry in the bottom of the helix bundle. Such “open” conformations were highly populated in the two amyloidogenic mutants, Glu34Lys and Phe71Tyr, while the non-amyloidogenic Leu159Arg showed an intermediate population distribution between the amyloidogenic variants and the WT. In addition, Trp8, which occupied a single conformation adjacent to Trp72 in the “bottom” aromatic cluster in WT, showed alternative conformations in Phe71Tyr and Leu159R but not in Glu34Lys. No alternative conformations were seen in Trp50 or Trp108 (Figure S3).

In summary, MD simulations suggested that alternative conformations of Trp72 (Figure 5) and perhaps Trp8 (Figure S3) at the bottom of the four-helix bundle could be responsible for the experimentally observed differences in Trp packing among the variant proteins (Figure 2B). On the basis of these observations, we propose that “open” conformations of Trp72, which were particularly highly populated in the two amyloidogenic variants, Glu34Lys and Phe71Tyr (Figure 5), could help initiate apoA-I misfolding by perturbing its structure at the bottom of the helix bundle. Such perturbations are expected to increase the level of solvent exposure of the nearby Tyr18 and other residues from the major amyloid hot spot Leu14–Leu22, thus favoring protein misfolding and amyloid formation.

DISCUSSION

This study allows new insights into the molecular events involved in apoA-I misfolding and amyloid formation. Usually, amyloidogenic mutations in globular proteins are destabilizing, which is thought to augment protein misfolding. Our biophysical data clearly show that Glu34Lys follows this general trend. The rank order of stability for the globular domain of apoA-I established in the current study is WT ≥ Phe71Tyr > Glu34Lys > Leu159Arg (Figure

2C). Notably, non-amyloidogenic Leu159Arg is the least stable variant explored so far. This paradoxical observation is consistent with our previous studies of full-length apoA-I using hydrogen–deuterium exchange mass spectrometry, which provided a molecular explanation for why the Leu159Arg variant is rapidly cleared *in vivo* rather than accumulating in amyloid.[19] Together, our studies show that structural destabilization *per se*, which can shift the balance between protein accumulation and clearance, is insufficient for amyloid deposition *in vivo*. Consequently, factors other than the overall decrease in the protein structural stability must be involved in AApoAI.[32–34] The study presented here helps identify additional factors contributing to apoA-I amyloid formation.

First, the low solubility of the full-length Glu34Lys apoA-I variant as compared to the solubilities of those investigated in our previous work suggests that this charge inversion augments protein aggregation. ApoA-I has a large fraction of charged residues that are nonrandomly distributed in amphipathic α-helices and are reported to form extensive stabilizing salt bridge networks.[13] In the crystal structure of the lipid-free WT globular domain, Glu34 does not form salt bridges and is separated by ~8 Å from the closest oppositely charged group, Lys45. Nevertheless, charge inversion in Glu34Lys, which is located in the hinge region at the top of the helix bundle, is expected to disrupt the overall electrostatic balance in this flexible region. Charged residues are key to apoA-I hydration,[35] which determines protein solubility and interactions with other molecules. Hence, charge inversion such as Glu34Lys is expected to alter electrostatic interactions not only among apoA-I molecules, thus altering protein solubility, but also between apoA-I and other molecules. For example, negatively charged heparan sulfate proteoglycans are expected to interact more favorably with the more electropositive Glu34Lys variant, potentially leading to an increased local concentration of the variant protein and augmenting its deposition in the extracellular matrix of tissues.[36] Although charge inversion may contribute to an increased level of aggregation of the Glu34Lys variant, this cannot fully explain its amyloidogenic behavior. In fact, of all known naturally occurring apoA-I variants containing Glu to Lys substitutions, which include Glu110Lys in sequence repeat h4 from the four-helix bundle, Glu136Lys in sequence repeat h5 from the flexible linker region, and Glu198Lys in sequence repeat h8 from the C-terminal tail (ref 37 and references therein), only Glu34Lys is amyloidogenic. Therefore, the location of the mutation site is paramount to the amyloidogenic outcome.

Second, our results suggest that transient opening of Trp72 represents a previously unidentified early step in the misfolding pathway of amyloidogenic variants of apoA-I, such as Glu34Lys. Indeed, we demonstrated experimentally that all apoA-I variants explored in this study have altered aromatic side chain packing in the globular domain (Figure 2B). Consistent with this finding, MD simulations suggested that WT and Glu34Lys, Phe71Tyr, and Leu159Arg apoA-I variants exist in a dynamic equilibrium between the “closed” and “open” Trp72 conformations and that the two AApoAI variants, Glu34Lys and Phe71Tyr, shift the equilibrium toward the “open” conformation (Figure 5). Such a shift is expected to facilitate the entry of water into the hydrophobic core of the helix bundle, thereby increasing the level of solvent exposure of major amyloid hot spot residues Leu14–Leu22 in apoA-I, which triggers protein misfolding. We posit that the mutation-sensitive molecular motions in

apoA-I (Figure 4), such as the dynamic opening and closing of the Trp72 side chain (Figure 5), may extend to other protein variants and influence their amyloidogenic behavior *in vivo*.

Our findings exemplify how diverse amino acid substitutions at various protein sites propagate across the molecule and alter protein conformation in sensitive regions, which can influence protein misfolding, proteolysis, and function. Indeed, amino acid substitutions in various apoA-I locations, including Glu34Lys (an “inside” mutation at the top of the helix bundle), Phe71Tyr (an “inside” mutation at its bottom), or Leu159Arg (an “outside” mutation near the middle), alter protein structure in similar regions, such as Trp72 at the bottom of the helix bundle (Figure 1). This phenomenon may extend to other apoA-I variants as well as to other globular proteins and their naturally occurring variants,[32] with potential implications for protein homeostasis and function in health and disease.

Supplementary Material

Refer to Web version on PubMed Central for supplementary material.

ACKNOWLEDGMENTS

The authors are indebted to Dr. Shobini Jayaraman (Boston University School of Medicine) for invaluable help throughout this project and Christopher J. Wilson (Northeastern University, Boston, MA) for performing intact mass check of recombinant proteins. The authors thank Dr. Xiaohu Mei (Boston University School of Medicine) for help during the early stages of protein expression.

Funding

This work was supported by the European Commission Marie Sklodowska Curie International Outgoing Fellowship, National Institutes of Health Grants RO1 GM067260 and RO1 GM107703, and the Stewart Family Amyloid Research Fund.

ABBREVIATIONS

apoA-I	apolipoprotein A-I
AApoAI	apoA-I amyloidosis
HDL	high-density lipoprotein
CD	circular dichroism
SEC	size-exclusion chromatography
MD	molecular dynamics
MBP	maltose binding protein

REFERENCES

(1). Nichols WC, Dwulet FE, Liepnieks J, and Benson MD (1988) Variant apolipoprotein AI as a major constituent of a human hereditary amyloid. Biochem. Biophys. Res. Commun. 156, 762–768. [PubMed: 3142462]

(2). Teoh CL, Griffin MD, and Howlett GJ (2011) Apolipoproteins and amyloid fibril formation in atherosclerosis. Protein Cell 2, 116–127. [PubMed: 21400045]

(3). Das M, and Gursky O (2015) Amyloid-forming properties of human apolipoproteins: Sequence analyses and structural insights. Adv. Exp. Med. Biol. 855, 175–211. [PubMed: 26149931]

(4). Rosenson RS, Brewer HB Jr., Davidson WS, Fayad ZA, Fuster V, Goldstein J, Hellerstein M, Jiang XC, Phillips MC, Rader DJ, Remaley AT, Rothblat GH, Tall AR, and Yvan-Charvet L (2012) Cholesterol efflux and atheroprotection: advancing the concept of reverse cholesterol transport. Circulation 125, 1905–1919. [PubMed: 22508840]

(5). Sorci-Thomas MG, Zabalawi M, Bharadwaj MS, Wilhelm AJ, Owen JS, Asztalos BF, Bhat S, and Thomas MJ (2012) Dysfunctional HDL containing L159R ApoA-I leads to exacerbation of atherosclerosis in hyperlipidemic mice. Biochim. Biophys. Acta, Mol. Cell Biol. Lipids 1821, 502–512.

(6). Obici L, Franceschini G, Calabresi L, Giorgetti S, Stoppini M, Merlini G, and Bellotti V (2006) Structure, function and amyloidogenic propensity of apolipoprotein A-I. Amyloid 13, 191–205. [PubMed: 17107880]

(7). Gillmore JD, Stangou AJ, Lachmann HJ, Goodman HJ, Wechalekar AD, Acheson J, Tennent GA, Bybee A, Gilbertson J, Rowczenio D, O'Grady J, Heaton ND, Pepys MB, and Hawkins PN (2006) Organ transplantation in hereditary apolipoprotein AI amyloidosis. Am. J. Transplant. 6, 2342–2347. [PubMed: 16925563]

(8). Rowczenio D, Dogan A, Theis JD, Vrana JA, Lachmann HJ, Wechalekar AD, Gilbertson JA, Hunt T, Gibbs SD, Sattianayagam PT, Pinney JH, Hawkins PN, and Gillmore JD (2011) Amyloidogenicity and clinical phenotype associated with five novel mutations in apolipoprotein A-I. Am. J. Pathol. 179, 1978–1987. [PubMed: 21820994]

(9). Gursky O, Mei X, and Atkinson D (2012) The crystal structure of the C-terminal truncated apolipoprotein A-I sheds new light on amyloid formation by the N-terminal fragment. Biochemistry 51, 10–18. [PubMed: 22229410]

(10). Mei X, and Atkinson D (2011) Crystal structure of C-terminal truncated apolipoprotein A-I reveals the assembly of high density lipoprotein (HDL) by dimerization. J. Biol. Chem. 286, 38570–38582. [PubMed: 21914797]

(11). Jayaraman S, Sanchez-Quesada JL, and Gursky O (2017) Triglyceride increase in the core of high-density lipoproteins augments apolipoprotein dissociation from the surface: Potential implications for treatment of apolipoprotein deposition diseases. Biochim. Biophys. Acta, Mol. Basis Dis. 1863, 200–210. [PubMed: 27768903]

(12). Mei X, Liu M, Herscovitz H, and Atkinson D (2016) Probing the C-terminal domain of lipid-free apoA-I demonstrates the vital role of the H10B sequence repeat in HDL formation. J. Lipid Res. 57, 1507–1517. [PubMed: 27317763]

(13). Segrest JP, Jones MK, Shao B, and Heinecke JW (2014) An experimentally robust model of monomeric apolipoprotein A-I created from a chimera of two X-ray structures and molecular dynamics simulations. Biochemistry 53, 7625–7640. [PubMed: 25423138]

(14). Gursky O (2013) Crystal structure of Δ(185–243)ApoA-I suggests a mechanistic framework for the protein adaptation to the changing lipid load in good cholesterol: from flatland to sphereland via double belt, belt buckle, double hairpin and trefoil/tetrafoil. J. Mol. Biol. 425, 1–16. [PubMed: 23041415]

(15). Melchior JT, Walker RG, Morris J, Jones MK, Segrest JP, Lima DB, Carvalho PC, Gozzo FC, Castleberry M, Thompson TB, and Davidson WS (2016) An evaluation of the crystal structure of C-terminal truncated apolipoprotein A-I in solution reveals structural dynamics related to lipid binding. J. Biol. Chem. 291, 5439–5451. [PubMed: 26755744]

(16). Melchior JT, Walker RG, Cooke AL, Morris J, Castleberry M, Thompson TB, Jones MK, Song HD, Rye KA, Oda MN, Sorci-Thomas MG, Thomas MJ, Heinecke JW, Mei X, Atkinson D, Segrest JP, Lund-Katz S, Phillips MC, and Davidson WS (2017) A consensus model of human apolipoprotein A-I in its monomeric and lipid-free state. Nat. Struct. Mol. Biol. 24, 1093–1099. [PubMed: 29131142]

(17). Chetty PS, Mayne L, Lund-Katz S, Englander SW, and Phillips MC (2017) Helical structure, stability, and dynamics in human apolipoprotein E3 and E4 by hydrogen exchange and mass spectrometry. Proc. Natl. Acad. Sci. U. S. A. 114 (5), 968–973. [PubMed: 28096372]

(18). Das M, Mei X, Jayaraman S, Atkinson D, and Gursky O (2014) Amyloidogenic mutations in human apolipoprotein A-I are not necessarily destabilizing - a common mechanism of

apolipoprotein A-I misfolding in familial amyloidosis and atherosclerosis. FEBS J. 281, 2525–2542. [PubMed: 24702826]

(19). Das M, Wilson CJ, Mei X, Wales TE, Engen JR, and Gursky O (2016) Structural stability and local dynamics in disease-causing mutants of human apolipoprotein A-I: What makes the protein amyloidogenic? J. Mol. Biol. 428, 449–462. [PubMed: 26562506]

(20). Andeen NK, Lam DY, de Boer IH, and Nicosia RF (2014) Renal ApoA-1 amyloidosis with Glu34Lys mutation and intraamyloid lipid accumulation. J. Am. Soc. Nephrol. 25, 2703–2705. [PubMed: 24925720]

(21). McManus DC, Scott BR, Franklin V, Sparks DL, and Marcel YL (2001) Proteolytic degradation and impaired secretion of an apolipoprotein A-I mutant associated with dominantly inherited hypoalphalipoproteinemia. J. Biol. Chem. 276, 21292–21302. [PubMed: 11292828]

(22). Mao D, and Wallace BA (1984) Differential light scattering and absorption flattening optical effects are minimal in the circular dichroism spectra of small unilamellar vesicles. Biochemistry 23 (12), 2667–2673. [PubMed: 6466606]

(23). Hoover WG (1985) Canonical dynamics: Equilibrium phase-space distributions. Phys. Rev. A: At., Mol., Opt. Phys. 31, 1695–1697.

(24). Nose,´ S. (1984) A unified formulation of the constant temperature molecular dynamics methods. J. Chem. Phys. 81, 511–519.

(25). Parrinello M, and Rahman A (1981) Polymorphic transitions in single crystals: A new molecular dynamics method. J. Appl. Phys. 52, 7182–7190.

(26). Jo S, Cheng X, Islam SM, Huang L, Rui H, Zhu A, Lee HS, Qi Y, Han W, Vanommeslaeghe K, MacKerell AD Jr., Roux B, and Im W (2014) CHARMM-GUI PDB manipulator for advanced modeling and simulations of proteins containing nonstandard residues. Adv. Protein Chem. Struct. Biol. 96, 235–265. [PubMed: 25443960]

(27). Jo S, Kim T, Iyer VG, and Im W (2008) CHARMM-GUI: A web-based graphical user interface for CHARMM. J. Comput. Chem. 29, 1859–1865. [PubMed: 18351591]

(28). Abraham M, Murtola T, Schulz R, Pall S, Smith J, Hess B, and Lindahl E (2015) GROMACS: High performance molecular simulations through multi-level parallelism from laptops to supercomputers. SoftwareX 1–2, 19–25.

(29). Best RB, Zhu X, Shim J, Lopes PE, Mittal J, Feig M, and Mackerell AD Jr. (2012) Optimization of the additive CHARMM all-atom protein force field targeting improved sampling of the backbone phi, psi and side-chain chi(1) and chi(2) dihedral angles. J. Chem. Theory Comput. 8, 3257–3273. [PubMed: 23341755]

(30). Humphrey W, Dalke A, and Schulten K (1996) VMD: Visual molecular dynamics. J. Mol. Graphics 14, 33–38.

(31). Michaud-Agrawal N, Denning EJ, Woolf TB, and Beckstein O (2011) MD Analysis: A toolkit for the analysis of molecular dynamics simulations. J. Comput. Chem. 32, 2319–2327. [PubMed: 21500218]

(32). Lucato CM, Lupton CJ, Halls ML, and Ellisdon AM (2017) Amyloidogenicity at a distance: How distal protein regions modulate aggregation in disease. J. Mol. Biol. 429, 1289–1304. [PubMed: 28342736]

(33). Stefl S, Nishi H, Petukh M, Panchenko AR, and Alexov E (2013) Molecular mechanisms of disease-causing missense mutations. J. Mol. Biol. 425 (21), 3919–3936. [PubMed: 23871686]

(34). Kucukkal TG, Petukh M, Li L, and Alexov E (2015) Structural and physico-chemical effects of disease and non-disease nsSNPs on proteins. Curr. Opin. Struct. Biol. 32, 18–24. [PubMed: 25658850]

(35). Benjwal S, and Gursky O (2010) Pressure perturbation calorimetry of apolipoproteins in solution and in model lipoproteins. Proteins: Struct., Funct., Genet. 78, 1175–1185. [PubMed: 19927327]

(36). Rosu SA, Rimoldi OJ, Prieto ED, Curto LM, Delfino JM, Ramella NA, and Tricerri MA (2015) Amyloidogenic propensity of a natural variant of human apolipoprotein A-I: stability and interaction with ligands. PLoS One 10, e0124946. [PubMed: 25950566]

(37). Takada Y, Sasaki J, Ogata S, Nakanishi T, Ikehara Y, and Arakawa K (1990) Isolation and characterization of human apolipoprotein A-I Fukuoka (110 Glu——Lys). A novel apolipoprotein variant. Biochim. Biophys. Acta, Lipids Lipid Metab. 1043 (2), 169–176.

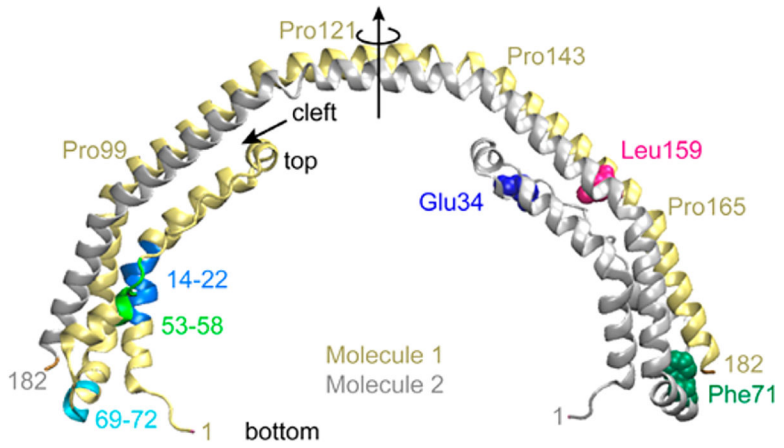

Figure 1.

Atomic structure of the globular domain of lipid-free human apoA-I. The 2.2 Å resolution X-ray crystal structure of free Δ(184–243) WT (Protein Data Bank entry 3R2P) shows a crystallographic dimer comprised of two helix bundles. Dimer molecules 1 (yellow) and 2 (gray) are related by a 2-fold symmetry axis (vertical arrow) that passes through the middle of the central linker (residues 121–142). Domain swapping around this flexible linker is thought to mediate monomer-to-dimer interconversion in apoA-I.[10,16] In the monomer (shown in Figure 3), all segments in the four-helix bundle are from the same molecule. The top and bottom of the bundle are indicated. A short arrow points to the hydrophobic cleft between two pairs of helices, which is proposed to open upon lipid binding. Mutated side chains explored in this study are shown in molecule 2 in a spherical representation: Glu34 (blue), Phe71 (green), and Leu159 (pink). Amyloid hot spots are shown in molecule 1 in residue segments 14–22 (blue), 53–58 (light green), and 69–72 (cyan).[18,19]

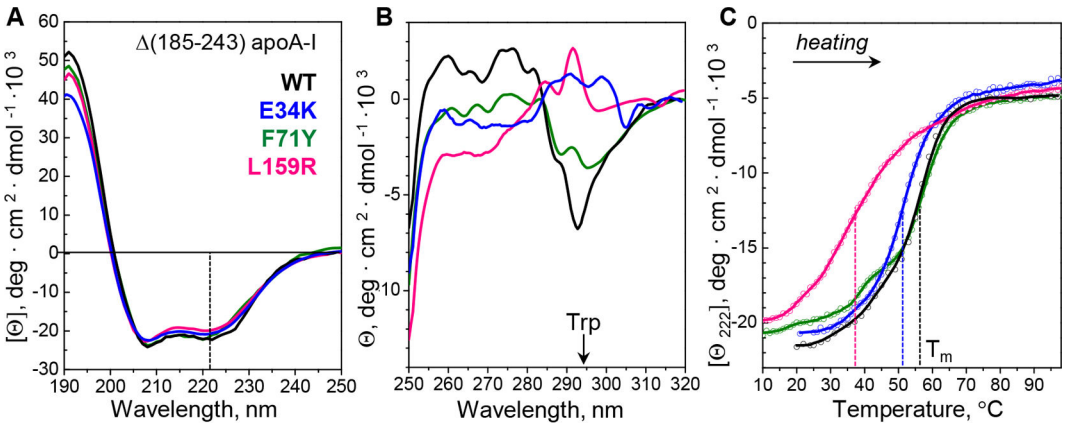

Figure 2.

Conformation and stability of recombinant C-terminally truncated proteins. Globular domains (residues 1–184) of WT (black), Glu34Lys (E34K, blue), Phe71Tyr (F71Y, green), and Leu159Arg (L159R, pink) were obtained and analyzed as described in Materials and Methods. (A) Far-UV CD spectra of the four proteins. Each spectrum represents three to five independent measurements. The helix content assessed from the CD signal at 222 nm (dashed line) ranged from 56 ± 5% in Leu159Arg to 62 ± 5% in WT. (B) Near-UV CD spectra of the four proteins show large differences, particularly at wavelengths dominated by Trp (a peak centered at ~295 nm, shown by an arrow). Each spectrum represents an average of three independent measurements with five-point adjacent averaging. (C) Melting data recorded by CD at 222 nm, $\Theta_{222}(T)$, monitor α-helical unfolding during heating. Circles show raw data points. Dashed lines indicate melting temperatures, T_m, corresponding to the first-derivative maxima, $d\Theta_{222}(T)/dT$.

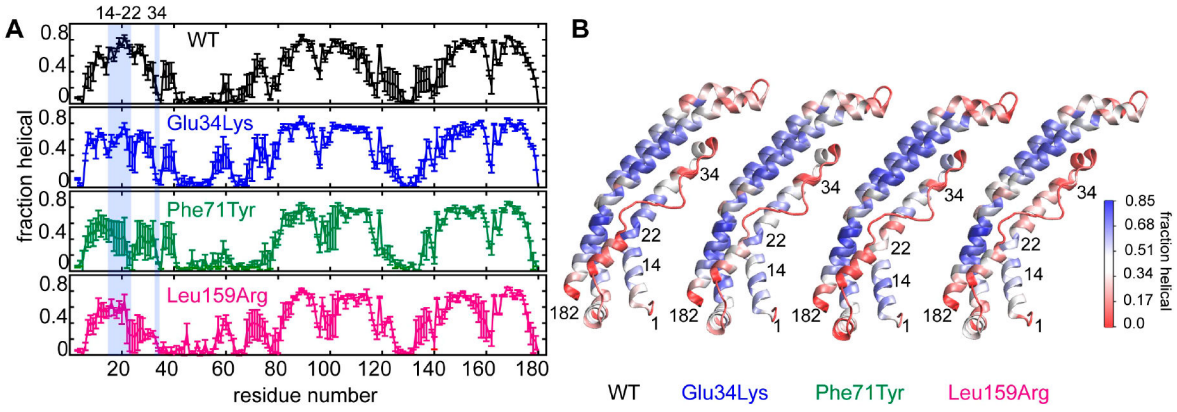

Figure 3.

Variations in the local helical conformation of WT, Glu34Lys, Phe71Tyr, and Leu159Arg proteins determined from high-temperature MD simulations. (A) Helical fraction vs residue number in apoA-I variants. WT and variant apoA-I are color-coded. For each protein, the dominant structure from the room-temperature simulations was heated to 500 K over 50 ps, followed by simulation for 20 ns at 500 K; the last 10 ns of these simulations was used to determine the helical fraction in each position. Standard errors of three replicates are shown by bars. The area shaded in blue depicts the major amyloidogenic hot spot residues, Leu14–Leu22, and the mutation site Glu34, as indicated by residue numbers at the top. (B) The starting structure for each protein is colored on the basis of the average helicity, from high to low helical fractions (blue to red, respectively), as indicated by the colored bar.

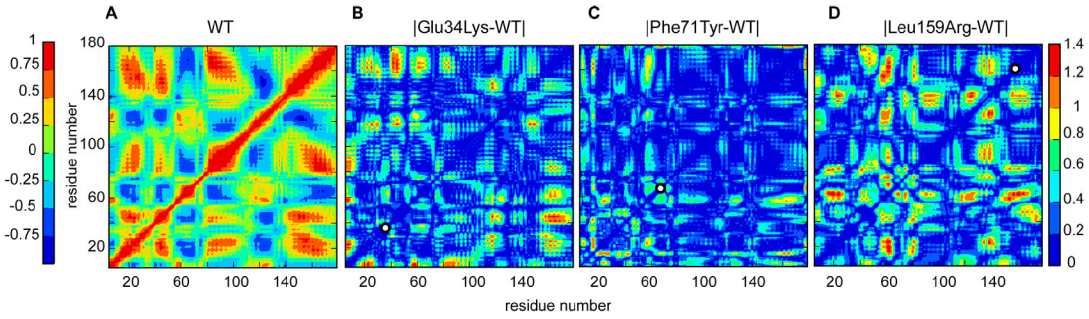

Figure 4.

Correlation maps illustrate concerted molecular motions in WT, Glu34Lys, Phe71Tyr, and Leu159Arg proteins. The maps were calculated over three independent high-temperature MD simulations. (A) Correlated molecular motions in WT depict protein groups that move either in concert (correlation coefficients from 0 to 1, green to red, respectively) or out of phase (0 to −1, teal to blue, respectively), as indicated in the left color bar. (B–D) Absolute difference between correlation maps of the three variants and WT apoA-I illustrating mutational effects on molecular motion. Groups whose relative motions remained invariant upon mutation are colored blue, and those whose correlated motions changed upon mutation are shown in warm colors (indicated in the right bar). The position of each apoA-I variant is marked with a white dot on the diagonal of each plot.

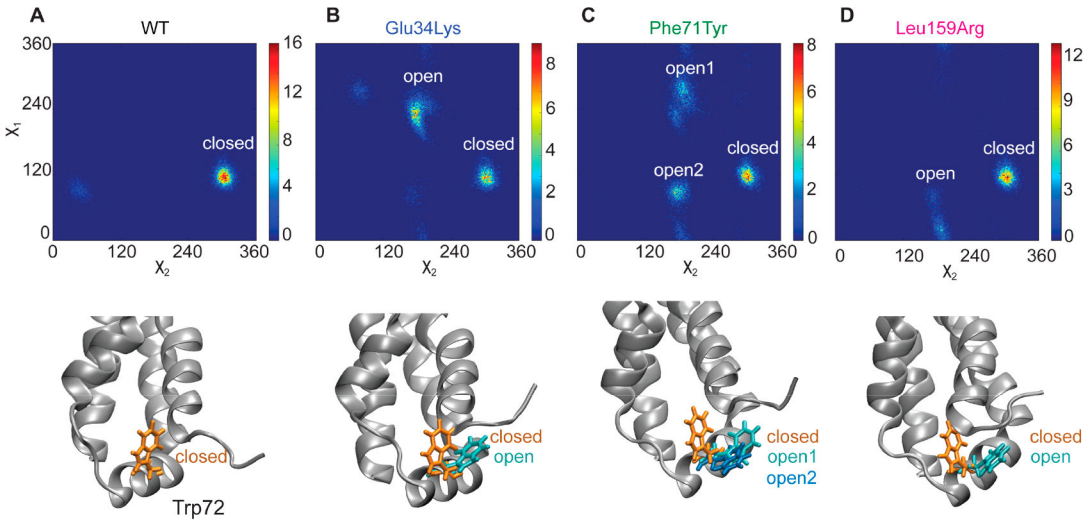

Figure 5.

Conformational distribution of the Trp72 side chain in WT and variant proteins. Probability distributions for dihedral angles χ_1 and χ_2 of Trp72 (top) and structural models depicting the corresponding conformations of the Trp72 side chain (bottom) in (A) WT, (B) Glu34Lys, (C) Phe71Tyr, and (D) Leu159Arg proteins. One representative result of three independent room-temperature simulations is shown. The probability is proportional to the number of steps in the simulation trajectory. Least and most probable conformations are colored blue and red, respectively, according to the color bars on the right. The color bars in different panels are different to illustrate the full range of probabilities for each protein. WT shows the sharpest peak corresponding to the “closed” Trp72 conformation. Glu34Lys, Phe71Tyr, and Leu159Arg proteins show additional peaks corresponding to “open” Trp72 conformations, which are depicted in the bottom panels. Stick models show “closed” (orange) and “open” (cyan and blue) orientations of the Trp72 side chain.